J. Anat. (2007) **210**, pp671–683 doi: 10.1111/j.1469-7580.2007.00724.x

REVIEW

Three-dimensional confocal morphometry – a new approach for studying dynamic changes in cell morphology in brain slices

Alexandr Chvátal,[1–3] Miroslava Anděrová[1,3] and Frank Kirchhoff[4]

[1]*Institute of Experimental Medicine, Academy of Sciences of the Czech Republic, Prague, Czech Republic*
[2]*Department of Neuroscience, Charles University, Second Medical Faculty, Prague, Czech Republic*
[3]*Center for Cell Therapy and Tissue Repair, Charles University, Prague, Czech Republic*
[4]*Department of Neurogenetics, Max Planck Institute of Experimental Medicine, Göttingen, Germany*

Abstract

Pathological states in the central nervous system lead to dramatic changes in the activity of neuroactive substances in the extracellular space, to changes in ionic homeostasis and often to cell swelling. To quantify changes in cell morphology over a certain period of time, we employed a new technique, three-dimensional confocal morphometry. In our experiments, performed on enhanced green fluorescent protein/glial fibrillary acidic protein astrocytes in brain slices *in situ* and thus preserving the extracellular microenvironment, confocal morphometry revealed that the application of hypotonic solution evoked two types of volume change. In one population of astrocytes, hypotonic stress evoked small cell volume changes followed by a regulatory volume decrease, while in the second population volume changes were significantly larger without subsequent volume regulation. Three-dimensional cell reconstruction revealed that even though the total astrocyte volume increased during hypotonic stress, the morphological changes in various cell compartments and processes were more complex than have been previously shown, including swelling, shrinking and structural rearrangement. Our data show that astrocytes in brain slices *in situ* during hypotonic stress display complex behaviour. One population of astrocytes is highly capable of cell volume regulation, while the second population is characterized by prominent cell swelling, accompanied by plastic changes in morphology. It is possible to speculate that these two astrocyte populations play different roles during physiological and pathological states.

Key words astrocytes; cell surface; cell volume; hypotonic stress.

Introduction

Astrocytes are the major glial cell population in the central nervous system (CNS) grey matter. It is believed that they play an important role in various processes during CNS development, the regulation of the extracellular concentrations of neuroactive substances, the maintenance of the extracellular space and during synaptic transmission (Hatten & Mason, 1990; Vernadakis, 1996; Ullian et al. 2001; Hansson & Ronnback, 2003; Kimelberg, 2004; Syková, 2005; Volterra & Meldolesi, 2005). The discovery of these many roles for glia in the healthy brain prompted researchers to reconsider their connection to diseases. It soon became evident that glial cells may have key roles in CNS disorders ranging from neuropathic pain and epilepsy to neurodegenerative diseases such as Alzheimer's and may even contribute to schizophrenia, depression and other psychiatric disorders (for reviews see Kimelberg et al. 1993; Miller, 2005). From the clinical point of view, any increase in

Correspondence
Alexandr Chvátal, PhD, DSc, Department of Cellular Neurophysiology, Institute of Experimental Medicine ASCR, Vídeňská 1083, 142 20 Praha 4, Czech Republic. T: +420 296 442670; F: +420 296 442783; E: chvatal@biomed.cas.cz

Accepted for publication *2 March 2007*

glial cell volume may represent a serious clinical problem because such an increase contributes to brain swelling and therefore to a rise in intracranial pressure, which often determines the fate of the patient (Kempski et al. 1991). Recent findings also indicate that neuroactive substances, ions and neurotransmitters released during neuronal activity or during pathological states into the extracellular space (ECS) interact with extrasynaptic receptors. Most of these receptors are present on glial cells, which respond to such stimulation by the activation of ion channels, second messengers and intracellular metabolic pathways. This in turn causes changes in glial volume, including the swelling and rearrangement of their processes, thus causing dynamic changes in ECS volume (for reviews see Syková & Chvátal 2000; Syková, 2005).

Studies of glial cell volume and glial morphometry

Currently, a number of techniques are employed to study glial cell volume changes and glial morphometry. Unfortunately, various methods to detect dynamic cell volume changes in cell cultures, i.e. recording intracellular changes in choline or tetramethylammonium (Ballanyi et al. 1990), measuring intracellular fluorescence intensity (Eriksson et al. 1992; Crowe et al. 1995; Aitken et al. 1998), imaging cells in transmitted light (Tomita et al. 1994; Aitken et al. 1998), scanning ion conductance (Korchev et al. 2000) or measuring pressure gradients (Davis et al. 2004), predominantly detect relative changes in cell volume and give little or no information about cell morphology. Recently, new real-time methods for evaluating cell volume changes in three dimensions (3D) have been established (Allansson et al. 1999; Boudreault & Grygorczyk, 2004). However, these methods were designed predominantly for cell cultures.

During the past decade, the 3D structure of astrocytes has been studied using various methods that have certain advantages and disadvantages. In studies utilizing electron microscopy, very fine morphological structures of astrocytes were determined (Kosaka & Hama, 1986; Grosche et al. 1999, 2002; Ogata & Kosaka, 2002; Hama et al. 2004). Unfortunately, using cell morphometry in these preparations may produce deviations from the real native shape and cell dimensions, because the tissue and its individual cellular elements are subjected to swelling during perfusion and dye injection, as well as shrinkage caused by fixation and embedding in the course of the procedure (Grosche et al. 2002). Indeed, it was shown in experiments in which unfixed, fixed and dehydrated myenteric neurons in the guinea-pig ileum were compared that there were only minor, insignificant changes in cell surface and volume during tissue fixation (Hanani et al. 1998). However, after dehydration and coversliping there were significant reductions along the major and minor axes of the cell body and significant decreases in the surface area and volume of the cells of 26.8 and 20.3%, respectively. The limitations of electron microscopy were partially solved by the 3D fluorescence imaging technique used to study the real-time effect of osmotic stress on astrocytes in cell cultures (Allansson et al. 1999); however, the disadvantages of this technique are its relatively low resolution, the computationally complex collection of the data and the possible phototoxic effect of the fluorescent dye. Recently, a new method was developed that allows the measurement of the cell volume, the cell surface area and the height of substrate-attached living cells, based on phase-contrast digital video microscopy (Boudreault & Grygorczyk, 2004). Even though this technique has good temporal resolution, with a typical time for single-image acquisition of around 100 ms, it was designed to study substrate-adherent cells only.

To overcome some of the limitations of the techniques mentioned above, 3D confocal cell morphometry was developed, which combines the high image resolution offered by confocal microscopy with an analysis of the time course of morphological changes of cells in living spinal cord and brain slices (Chvátal et al. 2007; Nepraśová et al. 2007). This technique combines intrinsic cell fluorescence in transgenic glial fibrillary acidic protein (GFAP)/enhanced green fluorescent protein (EGFP) mice together with confocal imaging, optical sectioning, morphometry and surface rendering. In the rest of the present overview, some advantages and disadvantages of this technique are discussed.

Transgenic animals – a new approach to the study of dynamic changes in cell morphology

Recently, transgenic mice in which astrocytes are labelled by EGFP under the control of the human GFAP promoter have been generated (Nolte et al. 2001). In experiments performed in the cortex, cerebellum, striatum, corpus callosum, hippocampus, retina and

spinal cord, co-labelling with antibodies against GFAP revealed an overlap with EGFP in the majority of cells and, in addition, EGFP-positive cells were negative for oligodendrocyte (MAG) and neuronal markers (NeuN). Two physiologically and morphologically distinct populations of astrocytes were identified: cells with numerous and highly branched processes (similar to protoplasmic astrocytes) expressing passive, non-inactivating potassium currents with a linear current–voltage relationship, and more simply shaped cells that are either bi- or tripolar, expressing predominantly voltage-gated, outwardly rectifying K^+ currents and small Na^+ inward currents, which are also characteristic of immature glial cells (Nolte et al. 2001). The properties of GFAP/EGFP astrocytes were recently analysed in a number of studies in the mouse brain *in situ* (Huttmann et al. 2003; Matthias et al. 2003; Grass et al. 2004; Hirrlinger et al. 2004; Wallraff et al. 2004; Jabs et al. 2005). In studies performed in acute hippocampal slices, however, two further types of GFAP/EGFP astrocytes were identified, distinguishable from each other by the expression of glutamate transporters (GluT cells) and ionotropic glutamate receptors (GluR cells) (Matthias et al. 2003; Wallraff et al. 2004; Jabs et al. 2005). GluT cells are extensively coupled via gap junctions and contact blood vessels, thus resembling classical astrocytes, whereas GluR cells lack junctional coupling and do not enwrap capillaries. In addition, GluR cells co-express S100β, a common astrocyte marker, NG2 and neuronal genes, and therefore are distinct from neurons, astrocytes and oligodendrocytes and were termed 'astrons' to indicate the intermediate status of these cells between neurons and glia (Matthias et al. 2003; Jabs et al. 2005). By contrast, the lack of the early neuronal marker TUC-4 in NG2-expressing EGFP-positive cells in acute brainstem slices suggests that these cells do not belong to a neuronally differentiated cell population, which in turn favours an astroglial relationship for these cells (Grass et al. 2004). The intrinsic fluorescence of GFAP/EGFP astrocytes is not toxic, and cell morphology can be studied in living brain slices, i.e. in a preserved extracellular microenvironment. It was shown in the morphometric study of Hirrlinger et al. (2004), using two-photon laser scanning microscopy in acutely isolated brainstem slices from GFAP/EGFP mice, that astroglial process endings displayed a high degree of dynamic morphological changes, suggesting their role in the direct modulation of synaptic transmission.

3D confocal morphometry reveals structural changes in astrocytes *in situ*

The time-course of changes in the cell morphology of astrocytes was studied using confocal 3D morphometry in brain cortex or spinal cord slices from transgenic GFAP/EGFP mice *in situ*, thus preserving the extracellular microenvironment (Chvátal et al. 2007; Nepraśová et al. 2007).

The image of a cell in an acute cerebral cortex slice *in situ* was sectioned along the vertical axis into a uniformly spaced set of 2D parallel images. Each pixel of the 2D image from each optical section was registered by a photomultiplier tube, digitized and recorded with information about the *xyz* size. This procedure resulted in a stack of consecutive 2D sectional images (Fig. 1A). Image processing and morphometric measurements were performed using the program CellAnalyst (Chvátal et al. 2007), comprising the following steps: (1) filtering of the images, including the removal of background noise, (2) thresholding and (3) morphometric calculations. The original images were improved using digital filtering techniques such as convolution and smoothing, which are routinely used in 3D cell reconstruction and morphometric procedures (for reviews see Blatter, 1999; Cox, 1999; Umesh Adiga & Chaudhuri, 2001). As a last step in the image-processing procedure, the background noise of the camera's CCD chip was removed (Fig. 1B), which was usually in the range of 2–10 in a 0–255 greyscale of the image. A threshold in the 0–255 greyscale, which affects which part of the image will be considered as a part of the cell, was determined by an interactive method that allows for the selection of a reasonable threshold under visual control. An area of the image in which the pixels had a value above the threshold and was therefore considered to be a part of the cell was selected in all parallel sections in a stack. Pixels at the border between above-threshold and below-threshold values were found in every image using an edge-detecting algorithm. Cell volumes were calculated using the Cavalieri method (Prakash et al. 1994; Kubinová et al. 1999; Duerstock et al. 2003; Mandarim-de-Lacerda, 2003). The cell surface was determined using the iso-contouring or iso-intensity contouring method (Kubinová et al. 1999; Duerstock et al. 2003). Three-dimensional surfaces of the cells were constructed based on the pixel value of the threshold, i.e. 'iso-values' (Fig. 1C). Changes in the complexity of the cell were determined by calculating the surface/volume

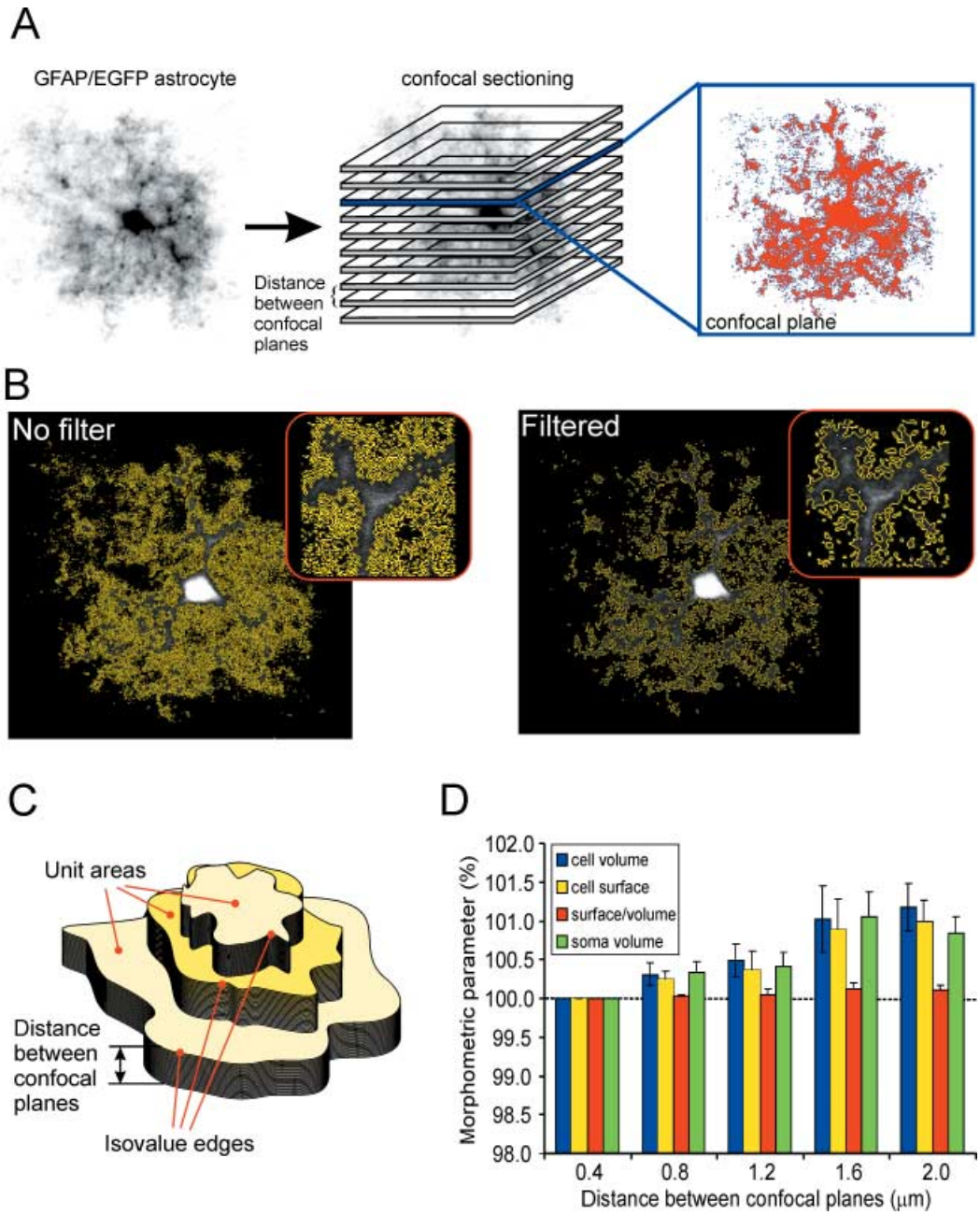

Fig. 1 Confocal morphometry of GFAP/EGFP astrocytes in brain slices. (A) Image of an astrocyte scanned using confocal microscopy, and obtained by volume rendering, i.e. recordings from all layers were superimposed. Parallel confocal planes superimposed on the astrocyte image indicate how a stack of images from a single cell was obtained. An example of a single image from one confocal plane showing a 2D cut through the astrocyte is shown in the inset. The image has been digitally filtered, and an area (marked by the red colour) of the image representing cellular structures is displayed. (B) Effect of the application of the digital filters shown in A. The border between the background (black) and the area of the image representing cellular structures is indicated by the yellow colour. Length values obtained from pixels indicating this border were used for calculating the cell surface area. (C) Scheme showing unit areas surrounded by isovalue edges and the distance between sections used for morphometric calculations. (D) Graph of the differences in morphometric parameters measured in a stack of images with different distances (0.4, 0.8, 1.2, 1.6 and 2.0 μm) between confocal planes. Morphometric values obtained using the smallest interlayer distance (0.4 μm) are plotted as 100%. Data from five cells that were scanned with an interlayer distance of 0.4 μm are shown. Stacks with larger distances were created from the original stacks by selecting every second image (0.8 μm), every third image (1.2 μm), every fourth image (1.6 μm) or every fifth image (2.0 μm).

(*S*/*V*) ratio, as was used in recent studies (Anděrová et al. 2004; Hama et al. 2004). The calculated value of a simple *S*/*V* ratio is, however, affected by the size of the object, and therefore to exclude interfering cell volume changes during osmotic stress, complexity (*C*) was calculated using $C = {}^{2}\sqrt{S}/{}^{3}\sqrt{V}$.

From images filtered using convolution kernels, whole-cell 3D object reconstructions of high-response astrocytes were constructed by rendering the cell surface (Chvátal et al. 2007). The 3D reconstructions were constructed based on images of intracellular fluorescence in GFAP/EGFP astrocytes that were filtered and thresholded, and therefore some fine processes and structures could not be visualized. However, all cell reconstructions showed a complex astrocytic structure: besides the cell soma, a number of cell domains connected to the soma by a simple process could be detected, the somatic membrane as well as cell domains had invaginations and protrusions, and some astrocytes had close connections with blood vessels (Fig. 2).

Confocal morphometry and morphology of astrocytes during hypotonic stress

The morphometry of cells obtained by confocal imaging may suffer from photobleaching. Our results show that the number of confocal sections through a cell may be adjusted to minimize the signal loss (Chvátal et al. 2007). An analysis of the morphological properties of GFAP/EGFP astrocytes in cerebral cortex slices *in situ* with an interlayer distance of 0.41 μm revealed that the average total cell volume of astrocytes was 14.68 ± 8.56 × 10^3 μm^3, the average cell surface area was 38.98 ± 1.82 × 10^3 μm^2 and the fraction represented by the cell soma was 14.63 ± 1.79% of the total cell volume (Table 1). The original sets of images were then reduced, and only images that corresponded to larger distances between sections were analysed. A distance between sections of 2.00 μm resulted in the number of images in a set being reduced to 50–60 in comparison with 200–250 when an interlayer distance of 0.41 μm was used (Fig. 1D). An analysis of the morphometric data obtained from sets of images with either 0.41 or 2.00 μm interlayer distances showed that the values for the cell volume, cell surface area and related parameters did not differ significantly. The morphometric data did not differ also when cell scanning was done using an interlayer distance of 1.51 μm, as shown in Table 2. These data show that the signal loss due to photobleaching during repetitive scans of the same cell over time can be reduced by increasing the interlayer distance.

Our analysis (Chvátal et al. 2007) revealed that a 20-min application of hypotonic solution (200 mmol kg^{-1}) evokes two types of reversible cell swelling (see also Fig. 3). In one population of astrocytes (low-response cells), hypotonic stress evokes a small increase in cell volume to 106.11% of control values (normalized to 100%), followed by a regulatory volume decrease. In the second population (high-response cells), the cell volume increase is significantly larger, up to 127.74%, without subsequent volume regulation. Low-response cells show a small increase in process volume to 105.46% of control values, while in high-response cells process swelling is significantly greater (135.12%). The astrocyte soma volume, expressed as a fraction of the total cell volume, increases during hypotonic stress in low-response cells to 104.99% of the control fraction values, while in high-response cells it decreases to 89.01%, indicating that the majority of the cell swelling seen during hypotonic stress in high-response astrocytes is due to the swelling of their processes. In contrast to low-response cells, the cell surface to volume ratio increases during hypotonic stress in high-response astrocytes to 104.05% of control values normalized to 100%, thus representing an increase in cell complexity.

Three-dimensional cell reconstruction before and after the application of the hypotonic stress (Fig. 4) revealed that even though the total astrocyte volume increases during hypotonic stress, the morphological changes in various cell compartments and processes are more complex than have been shown and include swelling, shrinkage and structural rearrangement (Chvátal et al. 2007).

Reliability of real-time confocal morphometry *in situ*

Besides the advantage of recording and analysing cell morphology over a certain period of time, there are, however, some limitations of confocal morphometry. The calculations of the morphometric parameters are based on intracellular fluorescence, and even though the original pictures are digitally improved, fine cell processes cannot be visualized. A recent study comparing 2D analysis of astrocytic processes performed using light microscopy (LM) and high-voltage electron microscopy (HVEM) revealed that the HVEM images of astrocytic processes were over two times more

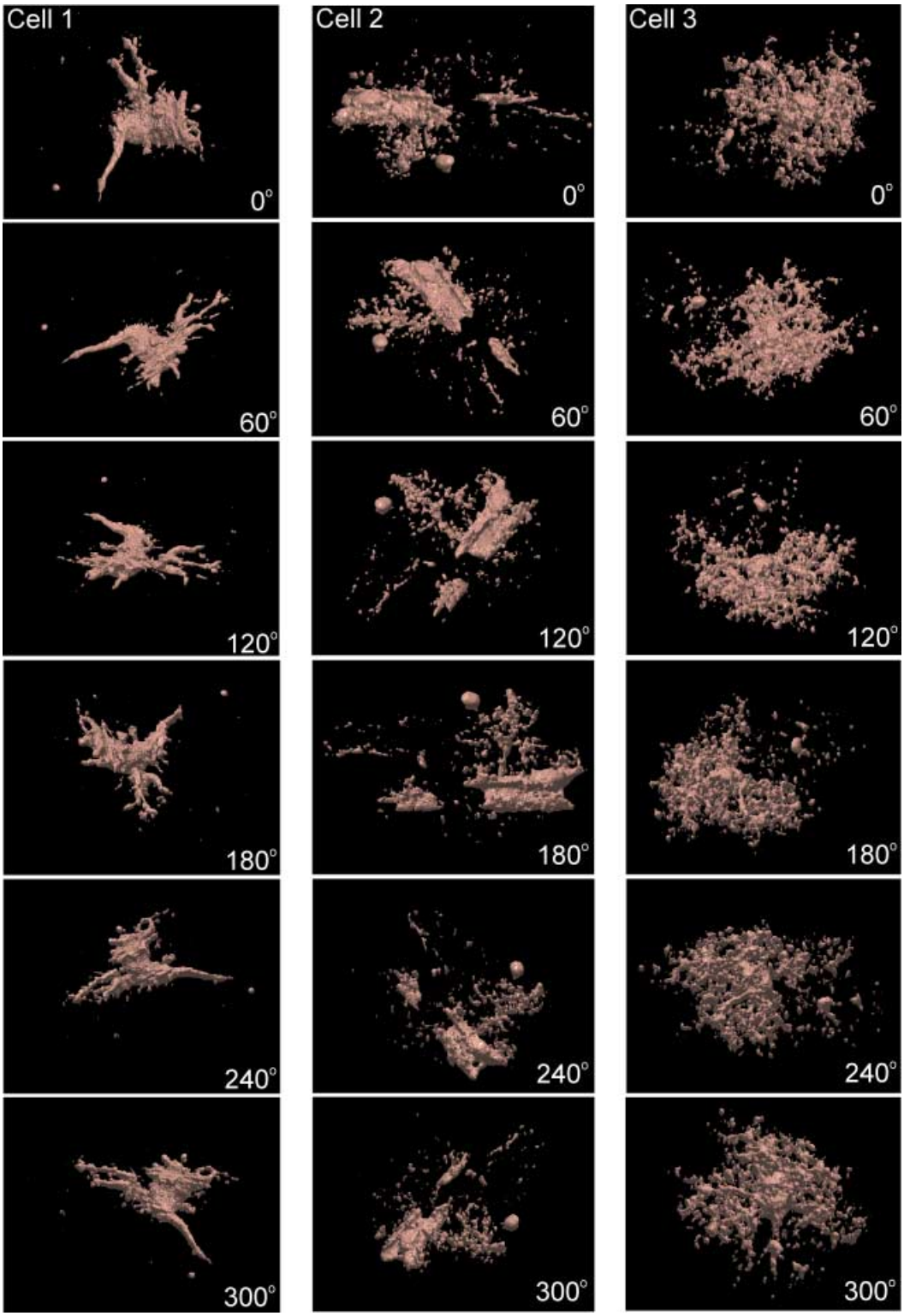

Fig. 2 Surface rendering of GFAP/EGFP astrocytes *in situ*. An example of surface rendering of three GFAP/EGFP astrocytes in brain slices. For 3D reconstruction, the same images filtered using convolution filters were used as for morphometric measurements. The rotation of the cells to a specific angle is indicated in each image.

Table 1 Morphometric parameters of GFAP/EGFP astrocytes calculated from a stack of images recorded with an interlayer distance of 0.4 μm

	V ($\mu m^3 \times 10^3$)	S ($\mu m^2 \times 10^3$)	$^2\sqrt{S}/^3\sqrt{V}$	V_s ($\mu m^3 \times 10^3$)	V_p ($\mu m^3 \times 10^3$)	V_s %	V_p %
Interlayer distance 0.4 μm							
Mean	14.68	38.98	8.06	2.12	12.56	14.63	85.37
SEM	0.86	1.82	0.17	0.25	0.86	1.79	1.79
Interlayer distance 2.0 μm							
Mean	14.86	39.37	8.07	2.14	12.72	14.59	85.41
SEM	0.91	1.89	0.16	0.25	0.91	1.80	1.80
n	5	5	5	5	5	5	5

Confocal scans of astrocytes were performed using an interlayer distance of 0.4 μm. For comparing morphometric calculations performed on image sets with different numbers of layers, data from the original image set were compared with a set in which the number of layers was reduced (interlayer distance 2.0 μm). Morphometric parameters were: V – total cell volume, S – cell surface area, surface to volume ratio expressed as $^2\sqrt{S}/^3\sqrt{V}$, V_s – soma volume, V_p – volume of cell processes, V_s % – soma volume as a percentage of the total cell volume, V_p % – process volume as a percentage of the total cell volume.

Table 2 Morphometric parameters of GFAP/EGFP astrocytes calculated from a stack of images with an interlayer distance of 1.5 μm

	V ($\mu m^3 \times 10^3$)	S ($\mu m^2 \times 10^3$)	$^2\sqrt{S}/^3\sqrt{V}$	V_s ($\mu m^3 \times 10^3$)	V_p ($\mu m^3 \times 10^3$)	V_s %	V_p %
All astrocytes							
Mean	14.71	36.13	7.71	2.91	11.79	21.64	78.36
SEM	1.33	3.05	0.20	0.33	1.23	2.59	2.59
n	21	21	21	21	21	21	21
Low-response astrocytes							
Mean	16.72	41.47	7.92	2.59	14.13	18.45	81.55
SEM	2.83	6.07	0.35	0.41	2.50	3.61	3.61
n	9	9	9	9	9	9	9
High-response astrocytes							
Mean	13.20	32.13	7.56	3.16	10.04	24.03	75.97
SEM	0.88	2.48	0.23	0.49	0.87	3.62	3.62
n	12	12	12	12	12	12	12

Morphometric parameters were: V – total cell volume, S – cell surface area, surface to volume ratio expressed as $^2\sqrt{S}/^3\sqrt{V}$, V_s – soma volume, V_p – volume of cell processes, V_s % – soma volume as a percentage of the total cell volume, V_p % – process volume as a percentage of the total cell volume.

complicated than the LM images (Hama et al. 2004). Photobleaching, which is potentially one of the critical sources of artefactual volume estimates (Blatter, 1999), is the other limitation of confocal morphometry. In our experiments (Chvátal et al. 2007; Nepraśová et al. 2007), photobleaching was reduced to a minimum by choosing the lowest excitation light intensity possible while still maintaining a reasonable signal-to-noise ratio in the acquired images, and by reducing the number of images in a stack by increasing the interlayer distance. The difference between morphometric data obtained in experiments with interlayer distances of 0.41 and 2.00 μm was less than 1.5%. Similar results were obtained in a study of phrenic motoneurons (Prakash et al. 1994), in which a sampling interval of 3.00 μm was found sufficient for estimating the mean phrenic motoneuron somal volume. Photobleaching observed in our experiments was linear, and therefore morphometric data obtained during extended measurements can be corrected for the signal decrease. Cell morphometric parameters such as surface area and volume are determined by iso-intensity countoring and

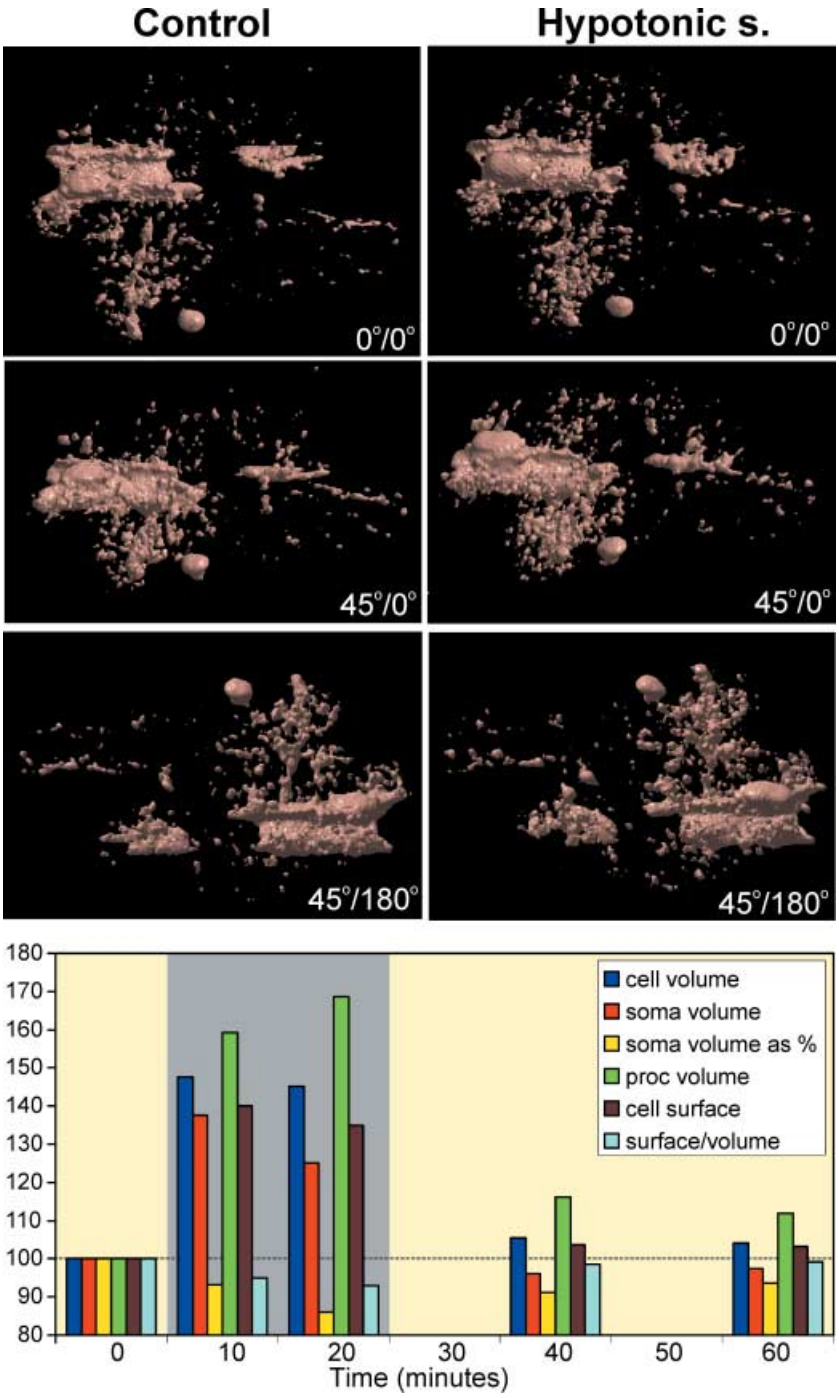

Fig. 3 Effect of hypotonic solution on the morphology and morphometric parameters of GFAP/EGFP astrocytes *in situ*. An example of morphological changes evoked by a 10-min application of hypotonic solution (200 mmol kg^{-1}) on a surface-rendered GFAP/EGFP astrocyte. Surface rendering of the astrocyte before the application of hypotonic solution (left) shows a complex cell morphology. Hypotonic solution (right) evoked an increase in total cell volume (swelling). Similarly, the volume of some cell compartments increased, while other cell compartments did not change and yet others decreased in volume or were rearranged. The graph shows the effect of a 20-min application of hypotonic solution (200 mmol kg^{-1}) on total cell volume, process volume, soma volume, soma volume expressed as a percentage of the total cell volume, cell surface area and the surface to volume ratio expressed as $^{2}\sqrt{S}/^{3}\sqrt{V}$ of the cell shown above. The time of application of the hypotonic solution is indicated by the grey rectangle. Graph was constructed using real-time relationships.

by the Cavalieri method, respectively. Some comparative studies (Kubinová et al. 1999; Duerstock et al. 2003) found no significant differences in comparison with other methods for surface area and volume estimation; however, the question of whether the calculated data are an accurate representation of the actual cell surface area and volume remains unanswered.

Morphological properties of GFAP/EGFP astrocytes

A 3D reconstruction of GFAP/EGFP astrocytes using surface rendering of filtered images shows a complex structure. Often a number of cell domains attached to the soma by a process can be observed, while some

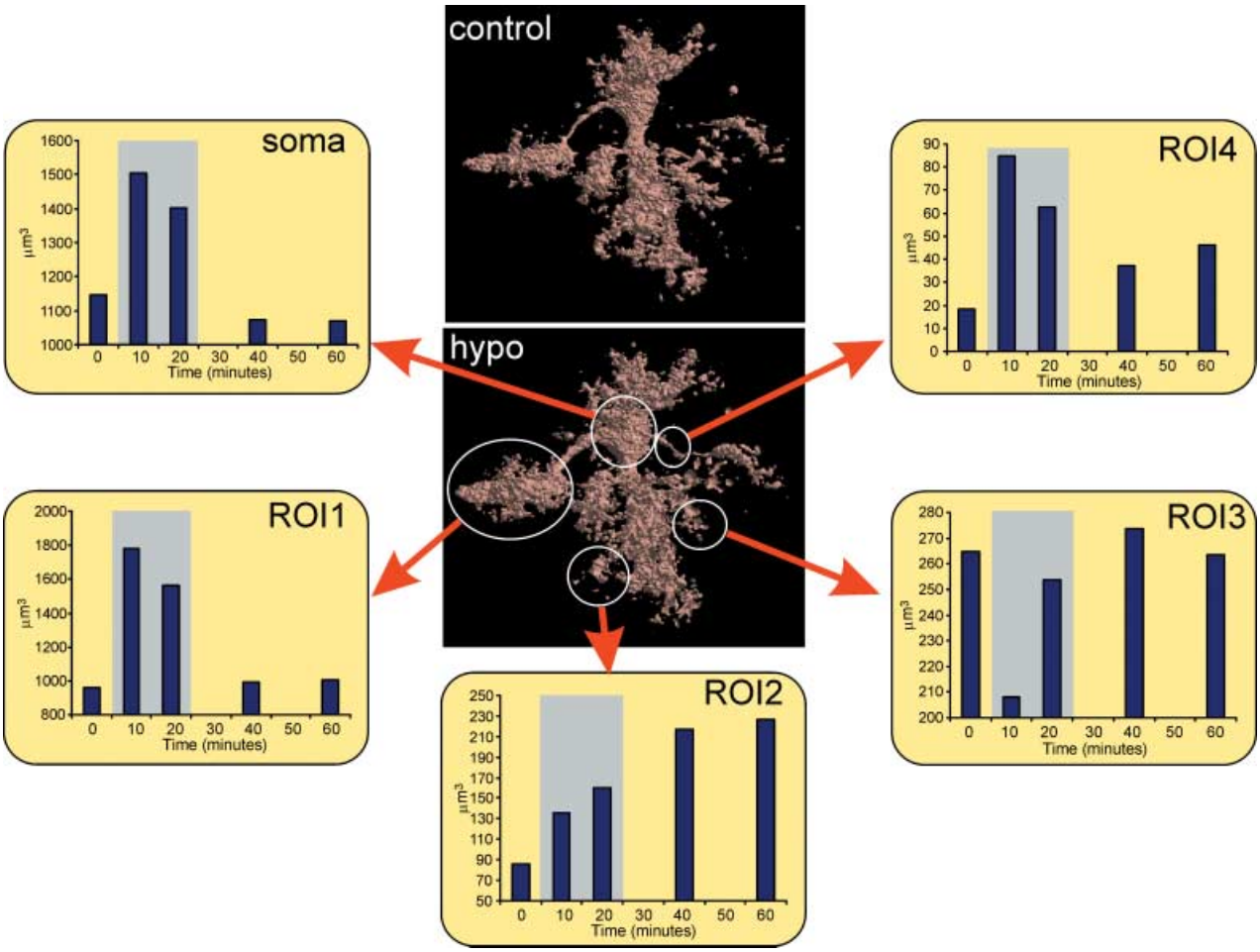

Fig. 4 Effect of hypotonic solution on the volume of GFAP/EGFP astrocyte compartments. The volume of the cell soma and various cell compartments during and after the application of hypotonic solution (200 mmol kg^{-1}). The following cell compartments were analysed: soma, cell domain attached to the cell soma by one process (ROI1), cell process directly attached to the soma (ROI4) and two distant cell processes (ROI2, ROI3). The time of application of the hypotonic solution is indicated by the grey rectangle. Data were normalized and corrected for the decrease in the signal produced by photobleaching. Graphs were constructed using real-time relationships.

astrocytes are attached to blood vessels. A complex cell structure was also observed in a study of the 3D structure of Bergmann glia using serial thin-section reconstructions (Grosche et al. 1999, 2002), in which glial appendages consisted of repetitive structural units termed 'microdomains'. It was shown that Bergmann glial cells may consist of hundreds of independent microdomains capable of limiting the spread of glial calcium elevations in response to underlying neuronal activity and therefore of autonomic interactions with groups of synapses that they contact. The 3D structure of GFAP/EGFP astrocytes in our experiments was constructed based on filtered and thresholded images of intrinsic intracellular fluorescence, and therefore some fine processes and structures could not be visualized and the cell complexity is probably underestimated. In addition, the cell membrane and cellular domains were not smooth, but had invaginations and protrusions, similar to the observations in morphological studies of unfixed myenteric neurons (Hanani et al. 1998).

As there are no previous direct measurements of the volume or surface area of living astrocytes in brain slices *in situ*, comparisons with published results are not possible. Nonetheless, some factors may affect the data obtained. For example, our measurements were performed at room temperature; however, we cannot exclude an effect of temperature, given that moderate hypothermia from 37 to 27 °C has been reported to cause rapid cell swelling with a maximum volume equal to 113% of the control volume being reached after

50 min (Plesnila et al. 2000). In fact, in comparison with studies in which the cell volume was determined in fixed tissue using electron microscopy, data obtained by confocal morphometry show a smaller cell volume. The volume of fluorescent-dye-labelled astrocytes in the stratum radiatum of the CA1 region in the dorsal hippocampus was estimated as 85.3×10^3 μm^3 (Ogata & Kosaka, 2002), and in measurements based on 3D segmented volumes the average astrocyte occupied a neuropilar volume of 65.9×10^3 μm^3 (Bushong et al. 2002), while in our experiments the average volume of GFAP/EGFP astrocytes in a living slice was 14.7×10^3 μm^3. Similarly, differences are also present when surface to volume ratios, indicating cell complexity, obtained using different techniques are compared. The average surface to volume ratio of astrocytic processes obtained using electron microscopy has been given as 13.0 μm^{-1} (Grosche et al. 1999, 2002) and 26.2 μm^{-1} (Hama et al. 2004), while in our experiments the surface to volume ratio of the whole cell was 2.64 μm^{-1}. Such differences may be due to cell swelling during the fixation procedure in electron microscopy measurements as well as to the differences in image processing and resolution between confocal and electron microscopy. Further detailed analysis is therefore necessary to validate the values of astrocyte volume and surface area in living brain tissue.

Morphological and volume changes in GFAP/EGFP astrocytes during osmotic stress

Morphological observations have shown that astrocytic swelling is the most pronounced cellular swelling in the grey matter in a number of pathological states (for reviews see Kimelberg, 2000, 2005). In our experiments we induced astrocytic swelling in brain slices via hypotonic stress. A similar approach has been used for many years to study processes associated with volume regulation in a wide variety of animals (Kimelberg et al. 1990). Also, increased extracellular K^+ has been used to induce astrocytic swelling in astrocyte cultures and brain slices, as extracellular K^+ is known to increase to levels of up to 80 mM during ischaemia (for review see Syková, 1983). However, increasing K^+ will introduce other effects, such as membrane depolarization, that could affect purely swelling-related phenomena.

In experiments performed in primary astrocyte cultures, exposure of cells to a hypotonic media leads to rapid cell swelling followed by the restoration of the cell volume towards normal values in the continued presence of hypotonic media, a process termed regulatory volume decrease or RVD (Kimelberg et al. 1990, 1993). In our experiments performed on astrocytes in brain slices *in situ*, hypotonic solution evoked two types of responses. In one population of cells it evoked little cell swelling, accompanied by RVD, while in the second, the volume increase was significantly greater and no RVD was observed. A similar diversity in the cellular response to hypotonic stress was also observed in freshly isolated rat hippocampal neurons (Aitken et al. 1998), where three types of cells were distinguished according to their responses: 'yielding cells' whose volume began to increase immediately, 'delayed response cells' that swelled after a latent period of 2 min or more and 'resistant cells' whose volume did not change during exposure to hypotonic solution. The soma and process compartments of the two types of astrocytes in our experiments also showed different behaviours. The volume of the astrocytic soma, expressed as a fraction of the total cell volume, increased during hypotonic stress in low-response cells, while in high-response cells it decreased, indicating that the majority of the cell swelling observed during hypotonic stress in high-response astrocytes is due to an increase in their process volume. Analogous compartmentalization has been found in fresh hippocampal slices, where neuronal cell body regions are resistant to osmotic swelling compared with their adjacent dendritic regions (Andrew et al. 1997).

Confocal morphometry data during hypotonic stress show that astrocytes are capable of dynamic and plastic changes in cell morphology. Three-dimensional cell reconstruction revealed that even though the total astrocyte volume increases, the morphology of different cell compartments changes in a complex manner, including swelling, shrinking and structural rearrangement. It is clear that findings showing that hypotonic solution produces a more rounded cell shape in experiments with cell cultures (Del Bigio et al. 1992; Tomita et al. 1994) should be re-evaluated. In the study of Del Bigio et al. (1992) performed on astroglia in suspension, during the initial period of severe swelling in hypotonic solution a decrease in the quantity and size of microvilli on the astroglial surfaces was observed. By contrast, we observed in our experiments an increase in cell complexity characterized by an increase in the surface to volume ratio in high-response cells. Similarly, different volume changes in various cell compartments were

observed in the study of Allansson et al. (1999), in which the volume of astroglial cells did not change uniformly throughout the cells, which also seemed to exhibit a varying capacity for regulating their volume.

A possible explanation for the plastic changes in processes and cell domains during hypotonic stress observed in our experiments as well as in the study of Hirrlinger et al. (2004) could be the involvement of the cell cytoskeleton. In addition, the process endings of GFAP/EGFP astrocytes at synaptic regions express a high degree of dynamic morphological changes (Hirrlinger et al. 2004), where two types of spontaneous motility can be distinguished, the gliding of thin lamellipodia-like membrane protrusions along neuronal surfaces and the transient extension of filopodia-like processes into the neuronal environment. In a study performed by Moran et al. (1996) on cultured astrocytes, swelling in response to hypotonic stress resulted in profound changes in the organization of the actin cytoskeleton. It was also observed in the same study that the organized network of microfilaments present under iso-osmotic conditions disappears with swelling and slowly recovers as volume regulation proceeds. Some experiments support the idea that astrocytes can undergo dramatic changes in their morphology, requiring the subcellular redistribution of most cytoskeletal proteins but without quantitative modifications in the amount of the respective proteins (Safavi-Abbasi et al. 2001). It was also suggested that receptor-mediated shape change in astroglial cells, observed in cultured astrocytes, occurs by a Ca^{2+}-independent mechanism that results in the active movement of the cytoplasm to the perinuclear region (Shain et al. 1992). This process is dependent on microtubule reassembly, suggesting that shape change may occur by the active movement of material along microtubules or by microtubule redistribution. On the other hand, the resistance to cell swelling observed in our experiments could protect the integrity of the membrane and its supporting structure and could also be explained by mechanical resilience, due in part or in whole to the support lent to the plasma membrane by the cytoskeleton (Aitken et al. 1998).

Changes in astrocyte morphology and diffusion in the extracellular space

The changes in glial morphology, especially in astrocytic processes, observed in our experiments in brain slices may be involved in changes of the extracellular diffusion parameters. The ECS is characterized by two parameters: the volume fraction, which represents the proportion of total tissue volume occupied by the ECS, and the tortuosity, which quantifies the hindrances imposed on the diffusion process by the tissue relative to an obstacle-free medium, i.e. it represents the barriers to the diffusion of neuroactive substances (for reviews see Nicholson & Syková, 1998; Nicholson, 2001; Hrabětová & Nicholson, 2004; Syková, 2005). There is experimental evidence that these two parameters are independent (Kume-Kick et al. 2002). It was also suggested by Syková et al. (1999) that swelling or thickening of fine cell processes, e.g. during astrogliosis, may decrease the overall volume of the ECS, but that additional diffusion barriers can still be formed. An example of the functional role of astrocytic processes in changes of diffusion barriers under physiological conditions has been shown in the supraoptic nucleus (SON) of the hypothalamus, where lactation triggered a withdrawal of astrocytic processes from the somatodendritic zone of the SON, which was interpreted by the authors as a removal of diffusion barriers leading to enhanced neuronal excitation and hormonal release (Piet et al. 2004). Similarly, Cashion et al. (2003) observed highly plastic astrocytes in young rats that exhibited time-of-day and oestrous cycle-related morphometric changes that may be involved in the preovulatory luteinizing hormone surge. It has been shown in a number of studies that tortuosity increases after astrogliosis induced in the rat spinal cord (Roitbak & Syková, 1999; Syková et al. 1999; Vargová et al. 2001) and in anaplastic astrocytomas in humans (Vargová et al. 2003). Due to intrinsic morphological properties, glial cells may also contribute to the formation of dead-space microdomains in the ECS under physiological and pathological conditions (Chen & Nicholson, 2000; Hrabětová & Nicholson, 2004). It has been proposed that diffusion in the CNS might be hindered not only by the size of the pores between the cells, but also by the cellular structure, including the fine swelling and movement of glial processes towards active synapses (Syková, 2005). Therefore, glial cells, in addition to their role in the maintenance of extracellular ionic homeostasis, may influence extracellular pathways for the diffusion of neuroactive substances in the brain.

Acknowledgements

This study was supported by grants of the Grant Agency of the Czech Republic, no. 305/06/1464 and no.

305/06/1316, by grants of the Czech Ministry of Education, Youth and Sports, no. 1M0538 and no. LC554, by a grant of the Czech Academy of Sciences, #AVOZ50390512, and by intramural funds of the Max-Planck-Society.

References

Aitken PG, Borgdorff AJ, Juta AJ, Kiehart DP, Somjen GG, Wadman WJ (1998) Volume changes induced by osmotic stress in freshly isolated rat hippocampal neurons. *Pflugers Arch* **436**, 991–998.

Allansson L, Khatibi S, Gustavsson T, Blomstrand F, Olsson T, Hansson E (1999) Single-cell volume estimation by three-dimensional wide-field microscopy applied to astroglial primary cultures. *J Neurosci Meth* **93**, 1–11.

Anděrová M, Antonova T, Petřík D, Neprašová H, Chvátal A, Syková E (2004) Voltage-dependent potassium currents in hypertrophied rat astrocytes after a cortical stab wound. *Glia* **48**, 311–326.

Andrew RD, Lobinowich ME, Osehobo EP (1997) Evidence against volume regulation by cortical brain cells during acute osmotic stress. *Exp Neurol* **143**, 300–312.

Ballanyi K, Grafe P, Serve G, Schlue WR (1990) Electrophysiological measurements of volume changes in leech neuropile glial cells. *Glia* **3**, 151–158.

Blatter LA (1999) Cell volume measurements by fluorescence confocal microscopy: theoretical and practical aspects. *Meth Enzymol* **307**, 274–295.

Boudreault F, Grygorczyk R (2004) Evaluation of rapid volume changes of substrate-adherent cells by conventional microscopy 3D imaging. *J Microsc* **215**, 302–312.

Bushong EA, Martone ME, Jones YZ, Ellisman MH (2002) Protoplasmic astrocytes in CA1 stratum radiatum occupy separate anatomical domains. *J Neurosci* **22**, 183–192.

Cashion AB, Smith MJ, Wise PM (2003) The morphometry of astrocytes in the rostral preoptic area exhibits a diurnal rhythm on proestrus: relationship to the luteinizing hormone surge and effects of age. *Endocrinology* **144**, 274–280.

Chen KC, Nicholson C (2000) Changes in brain cell shape create residual extracellular space volume and explain tortuosity behavior during osmotic challenge. *Proc Natl Acad Sci USA* **97**, 8306–8311.

Chvátal A, Anděrová M, Hock M, et al. (2007) Three-dimensional confocal morphometry reveals structural changes in astrocyte morphology in situ. *J Neurosci Res* **85**, 260–271.

Cox G (1999) Equipment for mass storage and processing of data. *Meth Enzymol* **307**, 29–55.

Crowe WE, Altamirano J, Huerto L, Alvarez-Leefmans FJ (1995) Volume changes in single N1E-115 neuroblastoma cells measured with a fluorescent probe. *Neuroscience* **69**, 283–296.

Davis CE, Rychak JJ, Hosticka B, et al. (2004) A novel method for measuring dynamic changes in cell volume. *J Appl Physiol* **96**, 1886–1893.

Del Bigio MR, Fedoroff S, Qualtiere LF (1992) Morphology of astroglia in colony cultures following transient exposure to potassium ion, hypoosmolarity and vasopressin. *J Neurocytol* **21**, 7–18.

Duerstock BS, Bajaj CL, Borgens RB (2003) A comparative study of the quantitative accuracy of three-dimensional reconstructions of spinal cord from serial histological sections. *J Microsc* **210**, 138–148.

Eriksson PS, Nilsson M, Wagberg M, Ronnback L, Hansson E (1992) Volume regulation of single astroglial cells in primary culture. *Neurosci Lett* **143**, 195–199.

Grass D, Pawlowski PG, Hirrlinger J, et al. (2004) Diversity of functional astroglial properties in the respiratory network. *J Neurosci* **24**, 1358–1365.

Grosche J, Matyash V, Moller T, Verkhratsky A, Reichenbach A, Kettenmann H (1999) Microdomains for neuron–glia interaction: parallel fiber signaling to Bergmann glial cells. *Nat Neurosci* **2**, 139–143.

Grosche J, Kettenmann H, Reichenbach A (2002) Bergmann glial cells form distinct morphological structures to interact with cerebellar neurons. *J Neurosci Res* **68**, 138–149.

Hama K, Arii T, Katayama E, Marton M, Ellisman MH (2004) Tri-dimensional morphometric analysis of astrocytic processes with high voltage electron microscopy of thick Golgi preparations. *J Neurocytol* **33**, 277–285.

Hanani M, Ermilov LG, Schmalz PF, Louzon V, Miller SM, Szurszewski JH (1998) The three-dimensional structure of myenteric neurons in the guinea-pig ileum. *J Auton Nerv Syst* **71**, 1–9.

Hansson E, Ronnback L (2003) Glial neuronal signaling in the central nervous system. *FASEB J* **17**, 341–348.

Hatten ME, Mason CA (1990) Mechanisms of glial-guided neuronal migration in vitro and in vivo. *Experientia* **46**, 907–916.

Hirrlinger J, Hulsmann S, Kirchhoff F (2004) Astroglial processes show spontaneous motility at active synaptic terminals in situ. *Eur J Neurosci* **20**, 2235–2239.

Hrabětová S, Nicholson C (2004) Contribution of dead-space microdomains to tortuosity of brain extracellular space. *Neurochem Int* **45**, 467–477.

Huttmann K, Sadgrove M, Wallraff A, et al. (2003) Seizures preferentially stimulate proliferation of radial glia-like astrocytes in the adult dentate gyrus: functional and immunocytochemical analysis. *Eur J Neurosci* **18**, 2769–2778.

Jabs R, Pivneva T, Huttmann K, et al. (2005) Synaptic transmission onto hippocampal glial cells with hGFAP promoter activity. *J Cell Sci* **118**, 3791–3803.

Kempski O, von Rosen S, Weigt H, Staub F, Peters J, Baethmann A (1991) Glial ion transport and volume control. *Ann NY Acad Sci* **633**, 306–317.

Kimelberg HK, Goderie SK, Higman S, Pang S, Cole R, Parsons DF (1990) Volume changes of astrocytes in vitro as a model for pathological astrocytic swelling. In *Differentiation and Function of Glial Cells* (ed. Levi G), pp. 335–348. New York: John Wiley & Sons, Inc.

Kimelberg HK, O'Connor ER, Kettenmann H (1993) Effects of swelling on glial cell function. *Adv Comp Environ Physiol* **14**, 157–186.

Kimelberg HK (2000) Cell volume in the CNS: regulation and implications for nervous system function and pathology. *Neuroscientist* **6**, 14–25.

Kimelberg HK (2004) Water homeostasis in the brain: basic concepts. *Neuroscience* **129**, 851–860.

Kimelberg HK (2005) Astrocytic swelling in cerebral ischemia as a possible cause of injury and target for therapy. *Glia* **50**, 389–397.

Korchev YE, Gorelik J, Laboratory MJ, et al. (2000) Cell volume measurement using scanning ion conductance microscopy. *Biophys J* **78**, 451–457.

Kosaka T, Hama K (1986) Three-dimensional structure of astrocytes in the rat dentate gyrus. *J Comp Neurol* **249**, 242–260.

Kubinová L, Janáček J, Guilak F, Opatrný Z (1999) Comparison of several digital and stereological methods for estimating surface area and volume of cells studied by confocal microscopy. *Cytometry* **36**, 85–95.

Kume-Kick J, Mazel T, Voříšek I, Hrabětová S, Tao L, Nicholson C (2002) Independence of extracellular tortuosity and volume fraction during osmotic challenge in rat neocortex. *J Physiol* **542**, 515–527.

Mandarim-de-Lacerda CA (2003) Stereological tools in biomedical research. *An Acad Bras Cienc* **75**, 469–486.

Matthias K, Kirchhoff F, Seifert G, et al. (2003) Segregated expression of AMPA-type glutamate receptors and glutamate transporters defines distinct astrocyte populations in the mouse hippocampus. *J Neurosci* **23**, 1750–1758.

Miller G (2005) Neuroscience. The dark side of glia. *Science* **308**, 778–781.

Moran J, Sabanero M, Meza I, Pasantes-Morales H (1996) Changes of actin cytoskeleton during swelling and regulatory volume decrease in cultured astrocytes. *Am J Physiol* **271**, C1901–C1907.

Neprašová H, Anděrová M, Petřík D, et al. (2007) High extracellular K^+ evokes changes in voltage-dependent K^+ and Na^+ currents and volume regulation in astrocytes. *Eur J Physiol* **453**, 839–849.

Nicholson C, Syková E (1998) Extracellular space structure revealed by diffusion analysis. *Trends Neurosci* **21**, 207–215.

Nicholson C (2001) Diffusion and related transport mechanisms in brain tissue. *Rep Prog Phys* **64**, 815–884.

Nolte C, Matyash M, Pivneva T, et al. (2001) GFAP promoter-controlled EGFP-expressing transgenic mice: a tool to visualize astrocytes and astrogliosis in living brain tissue. *Glia* **33**, 72–86.

Ogata K, Kosaka T (2002) Structural and quantitative analysis of astrocytes in the mouse hippocampus. *Neuroscience* **113**, 221–233.

Piet R, Vargová L, Syková E, Poulain DA, Oliet SH (2004) Physiological contribution of the astrocytic environment of neurons to intersynaptic crosstalk. *Proc Natl Acad Sci USA* **101**, 2151–2155.

Plesnila N, Muller E, Guretzki S, Ringel F, Staub F, Baethmann A (2000) Effect of hypothermia on the volume of rat glial cells. *J Physiol* **523**, 155–162.

Prakash YS, Smithson KG, Sieck GC (1994) Application of the Cavalieri principle in volume estimation using laser confocal microscopy. *Neuroimage* **1**, 325–333.

Roitbak T, Syková E (1999) Diffusion barriers evoked in the rat cortex by reactive astrogliosis. *Glia* **28**, 40–48.

Safavi-Abbasi S, Wolff JR, Missler M (2001) Rapid morphological changes in astrocytes are accompanied by redistribution but not by quantitative changes of cytoskeletal proteins. *Glia* **36**, 102–115.

Shain W, Bausback D, Fiero A, Madelian V, Turner JN (1992) Regulation of receptor-mediated shape change in astroglial cells. *Glia* **5**, 223–238.

Syková E (1983) Extracellular K^+ accumulation in the central nervous system. *Prog Biophys Mol Biol* **42**, 135–189.

Syková E, Vargová L, Prokopová S, Šimonová Z (1999) Glial swelling and astrogliosis produce diffusion barriers in the rat spinal cord. *Glia* **25**, 56–70.

Syková E, Chvátal A (2000) Glial cells and volume transmission in the CNS. *Neurochem Int* **36**, 397–409.

Syková E (2005) Glia and volume transmission during physiological and pathological states. *J Neural Transm* **112**, 137–147.

Tomita M, Fukuuchi Y, Terakawa S (1994) Differential behavior of glial and neuronal cells exposed to hypotonic solution. *Acta Neurochir (Suppl) (Wien)* **60**, 31–33.

Ullian EM, Sapperstein SK, Christopherson KS, Barres BA (2001) Control of synapse number by glia. *Science* **291**, 657–661.

Umesh Adiga PS, Chaudhuri BB (2001) Some efficient methods to correct confocal images for easy interpretation. *Micron* **32**, 363–370.

Vargová L, Jendelová P, Chvátal A, Syková E (2001) Glutamate, NMDA, and AMPA induced changes in extracellular space volume and tortuosity in the rat spinal cord. *J Cereb Blood Flow Metab* **21**, 1077–1089.

Vargová L, Homola A, Zámečník J, Tichý M, Beneš V, Syková E (2003) Diffusion parameters of the extracellular space in human gliomas. *Glia* **42**, 77–88.

Vernadakis A (1996) Glia–neuron intercommunications and synaptic plasticity. *Prog Neurobiol* **49**, 185–214.

Volterra A, Meldolesi J (2005) Astrocytes, from brain glue to communication elements: the revolution continues. *Nat Rev Neurosci* **6**, 626–640.

Wallraff A, Odermatt B, Willecke K, Steinhauser C (2004) Distinct types of astroglial cells in the hippocampus differ in gap junction coupling. *Glia* **48**, 36–43.